# Efficient Lateral Electron Transport inside a Monolayer of Aromatic Amines Anchored on Nanocrystalline Metal Oxide Films

**Pierre Bonhôte,* Eric Gogniat, Sophie Tingry, Christophe Barbé, Nicolas Vlachopoulos, Frank Lenzmann, Pascal Comte, and Michael Grätzel**

*Laboratoire de photonique et interfaces, Département de chimie, Ecole Polytechnique Fédérale de Lausanne, CH-1015 Lausanne, Switzerland*

*Received: September 4, 1997; In Final Form: December 17, 1997*

A monolayer of a phosphonated triarylamine adsorbed on nanocrystalline $TiO_2$, $ZrO_2$, or $Al_2O_3$ film deposited on conducting glass displays reversible electrochemical and electrochromic behavior although the redox potential of the electroactive molecules (0.80 V vs NHE) lies in the forbidden band of the semiconducting or insulating oxides. The mechanism of charge transport was found to involve hole injection from the conducting support followed by lateral electron hopping within the monolayer. The apparent diffusion coefficient ranged from $2.8 \times 10^{-12}$ m$^2$ s$^{-1}$ in the neat 1-ethyl-2-methylimidazolium bis(trifluoromethylsulfonyl)imide ($EtMeIm^+Tf_2N^-$) to $1.1 \times 10^{-11}$ m$^2$ s$^{-1}$ in acetonitrile + 2 M $EtMeIm^+Tf_2N^-$. A percolation threshold for electronic conductivity was found at a surface coverage corresponding to 50% of a full monolayer.

## Introduction

Nanocrystalline semiconductor films, in particular of $TiO_2$, are a proven and very versatile component[1] in the fabrication of dye-sensitized solar cells,[2] electrochromic devices,[3] and sensors,[4] as well as photoelectrosynthetic[5] or photoelectrochromic[6] cells, owing to their unique properties of high surface area, transparency, and electronic conductivity. However, based on the existence of an electronic band gap in the material, it was assumed until now that interfaces to the nanocrystalline semiconductor layers are conductive only in the accumulation regime and are electronically blocking under reverse bias. Thus, charge-transfer reactions should be restricted to adsorbed species whose redox potential lies above the conduction band edge. For $TiO_2$, the flat band potential ($V_{fb}$) in aprotic solvents such as $CH_3CN$ is very negative (as far as − 2 V)[7] but can be raised to 0 V by addition of $Li^+$.[3] Thus, surface-anchored viologens such as **3** ($E^\circ = -0.4$ V) display a reversible behavior only in the presence of $Li^+$. In the absence of lithium ions, the reduction is irreversible.

In view of this fact, it was striking to observe that compound **1** did exhibit reversible electrochemistry when grafted onto nanocrystalline $TiO_2$ layers supported by conducting glass, even though its redox potential (0.80 V) is located in a domain where the $TiO_2$ interface is expected to be blocking. The phosphonated tetraalkyl-*p*-phenylenediamine **2** ($E^\circ = 0.28$ V) also displays electroactivity but in a much weaker and less reversible fashion.

Three electron transport mechanisms can in principle be proposed to explain the observed electroactivity. First, the electrons could be carried by the supporting semiconductor. Second, they could be transported by the triarylamine molecules in a diffusive process. Third, they could be transported by the triarylamine molecules in an electron hopping process. The first hypothesis implies that an electron flow can exist on the semiconductor surface, in the middle of the band gap, by hopping from surface state to surface state. Such a mechanism, even though it cannot be ruled out on a theoretical basis, is very unlikely in the present case, as the same electroactivity of **1** as a monolayer was observed on nanocrystalline aluminum oxide layers. It appears thus that the electrons are transported by the triarylamine **1**. In such a case, the second and the third mechanism can be implicated. In the second hypothesis, the triarylamine molecules should be sufficiently mobile inside the monolayer or between the monolayer and the contacting solution, to account for a diffusive electron transport to the underlying conducting glass. In the third hypothesis, the molecules should be firmly enough bound to the metal oxide surface to prevent significant diffusion, and charge motion could only take place by electron hopping between molecules inside the monolayer. These two types of electron transport, which often coexist in a given material, were extensively studied for various types of electroactive materials deposited on electrodes[8] and were the subject of extensive theoretical descriptions and simulations by Blauch and Savéant.[9] Diffusive and hopping charge transport exhibit very different behavior. Ideally, in a purely diffusive process, the apparent diffusion coefficient $D_{app}$ of the electroactive species should be independent of the concentration of that species in the considered material. Practically, structural changes often lead to a decrease in $D_{app}$ with increasing concentration.[10] Moreover, the conductivity remains even at low concentration. On the contrary, in an electron hopping process, $D_{app}$ increases with the concentration $C$ of the electroactive species, as expressed by the Dahms−Ruff (DR)[11] and the Laviron−Andrieux−Savéant (LAS)[12] equations (eq 1), in which $k_{ex}$ is the electron self-exchange rate constant and $\delta$ the intermolecular distance at which the electron transfer takes place.

$$D_{app} = k_{ex}\delta^2 C/6 \qquad (1)$$

The meaning of $\delta$ is slightly different in the DR and in the LAS equation which apply to redox centers that are respectively freely diffusing and linked to a backbone with a restricted motion freedom around an equilibrium position. None of these two models describe an assembly where the redox centers are completely immobilized and where the electron transfer does not require molecular displacement. In such an extreme case,

S1089-5647(97)02890-3 CCC: $15.00 
Published on Web 02/10/1998

classical percolation behavior is expected, characterized by a sharp threshold below which the conductivity drops to zero as the contact between the electroactive centers breaks down. If, however, the electron hopping is not strictly restricted to adjacent redox sites, the predicted transition at the percolation limit is softer, and $D_{app}$, even if minute, is not nil below that limit.[9b]

To our knowledge, the only study on electron transport inside a monolayer of electroactive molecules on a mesoporous material was carried out by Majda and co-workers on an aluminum oxide film in which 80 nm wide pores were organized perpendicularly to a gold support. The alumina was derivatized with various polymers[13] or bilayers bearing redox active centers.[14] In all those cases, the observed conductivity was essentially due to the diffusion of the loosely bound charge carriers in the polymer or in the bilayer. For the latter structure, the apparent diffusion coefficient was reported to be independent of the concentration of electroactive species. Even though the supporting material was not nanocrystalline as in the present study, the structures of Majda's electrodes and of ours are similar, from the fact that in both systems a monolayer of electroactive molecules is organized on average perpendicularly to a conductive support, on the inner side of mesopores. Comparison between the systems is hence relevant.

An example of modified electrodes where conductivity occurs only by electron hopping was described by Anson et al.[15] The investigated system consisted of a poly(vinylpyridine) film on a conducting support, loaded with coordinately linked $Fe(CN)_5$ redox units, whose diffusion is negligible. When the concentration of $Fe(CN)_5$ was varied, a percolation threshold appeared, below which the electroactive fraction of the redox centers sharply dropped to zero. Two-dimensional percolation behavior was observed by Majda et al.[16] in a Langmuir monolayer of an osmium complex diluted by 1-octadecanol at the water surface. The apparent diffusion coefficient decreased rapidly from 2.4 $\times$ $10^5$ $m^2$ $s^{-1}$ to 0 as the mole fraction of the electroactive species was reduced from 1 to 0.6.

In the present work, electro- and spectroelectrochemical experiments were carried out on nanocrystalline electrodes derivatized by **1** in order to allow discrimination between a diffusive and an electron hopping mechanism of charge transport.

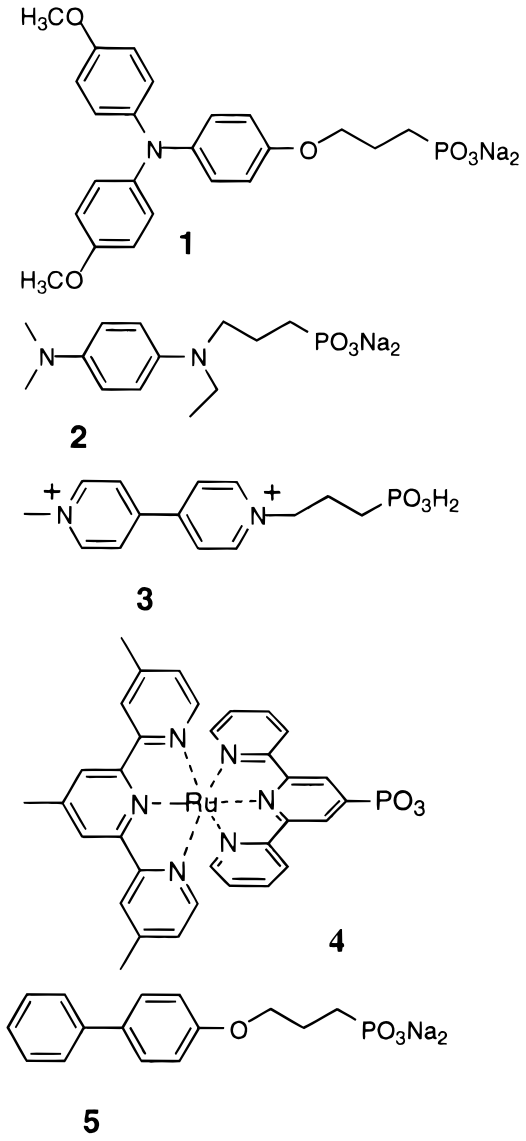


## Experimental Section

Reagents were purchased from Fluka, unless otherwise stated. Acetonitrile, ethanol, acetic acid, and cyclohexane were puriss, and the supporting electrolytes were electrochemical grade quality. Propylene carbonate was obtained from Burdick & Jackson. *tert*-Butyl methyl ether (hereafter TBME) was obtained from Siegfried. These compounds were not submitted to further purification before use. 3-Methoxypropionitrile was distilled over a Fischer HMS500 column.

**Electrochemistry.** Potentials are given vs NHE. Cyclic voltammetric and chronocoulometric experiments were carried out with a PC-controlled Ecochemie model Autolab P20 potentiostat. In all the experiments, the reference electrode was $Ag/Ag^+$-saturated NaCl (+0.197 V vs NHE), and the counter electrode was glassy carbon. Both were separated by a salt bridge from the solution in contact with the working electrode. For cyclic voltammetry, the working electrodes were a 4.8 $\mu$m film of $TiO_2$ on a 1 $cm^2$ conducting oxide substrate ($SnO_2$) derivatizated in 0.5 mM solutions in EtOH for 12−15 h at room temperature (r.t.). The electrolytic solution was 0.2 M tetrabutylammonium triflate in propylene carbonate. The spectrophotometric measurements were carried out with a HP8453 diode array spectrophotometer from Hewlett-Packard, in a 1 cm by 1 cm spectroelectrochemical cell.

Dynamic viscosity measurements were carried out on a Haake VT500 microviscosimeter, thermally controlled by a Haake D8 thermostat−cryostat.

$^1$H NMR spectra were recorded on a Bruker Spectrospin 200 MHz spectrometer.

Data processing and curve fitting were done with the help of the Igor Pro software form Wave Metrics Inc.

**Synthesis.** Synthesis of **1**, **4**, and **5** will be reported elsewhere. Synthesis of **3** is reported in ref 3c. All gave $^1$H NMR spectra consistent with their expected structure and free of foreign signals. Unless otherwise stated, the $^1$H NMR spectra given below were recorded in $CDCl_3$ with TMS as an internal standard, and the chemical shifts are given in ppm versus this reference. Diazabicylcooctane ($\delta = 2.83$) was added to protect the *p*-phenylenediamines from oxidation by air.

***N*-Ethyl-*N*′,*N*′-dimethyl-*p*-phenylenediamine.** In a dry, three-necked, round-bottomed flask equipped with a reflux condenser, a thermometer, and a magnetical stirrer, under Ar, *N*,*N*-dimethyl-*p*-phenylenediamine (4.08 g, 30 mmol) was dissolved in 300 mL of dry THF. The solution was cooled to −65 °C, and *n*-butyllithium (10 M in hexane, 3.2 mL, 32 mmol) was slowly added under stirring, keeping the temperature below

−60 °C. After 15 min at −65 °C, bromoethane (3.24 g, 30 mmol) was added in one portion. The mixture was allowed to warm to r.t. and then heated to 50 °C for 1 h. The solution was concentrated to 10 mL, diluted to 100 mL with heptane, and washed twice with water. This water was extracted with dichloromethane (2 × 50 mL). The combined organic phases were dried over $MgSO_4$ and concentrated to 10 mL. The concentrate was purified by chromatography over silica gel, eluting by heptane followed by heptane/TBME (4:1). The fraction eluted first gave a $R_f = 0.58$ by TLC on silica gel with TBME as eluent. The second one, with $R_f = 0.47$, was concentrated to 50 mL and cooled to −30 °C. The red crystals formed were filtered below 0 °C and dried under 12 mbar. The product is liquid at 20 °C and was kept in the solid state at −20 °C. Yield: 2.85 g (58%). *Caution: N*-ethyl-*N*′,*N*′-dimethyl-*p*-phenylenediamine is strongly irritating to the skin and must be handled with gloves. $^1$H NMR: 6.74 (dt, 2H, $J$ = 9 and 2.7 Hz), 6.60 (dt, 2H, $J$ = 9 and 2.7 Hz), 3.10 (q, 2H, $J$ = 7 Hz), 2.81 (s, 6H), 1.22 (t, 3H, $J$ = 7 Hz).

**Diethyl 3-(Ethyl(*p*-(*N*,*N*-dimethylamino)phenyl)amino)-propyl-1-phosphonate.** *N*-Ethyl-*N*′,*N*′-dimethyl-*p*-phenylenediamine (0.656 g, 4 mmol), diethyl 3-bromopropyl-1-phosphonate (1.04 g, 4 mmol), and 0.1 mL of *sym*-collidine were dissolved in acetonitrile (20 mL). The solution was refluxed for 3 h. Silica gel (1.5 g) was added, and the solvent was removed by a Rotavapor. The remaining solid was suspended in TBME and placed on the top of a silica gel chromatography column. Elution was done with TBME. The starting amine was eluted first ($R_f = 0.63$ by TLC on silica gel with acetone as eluent) followed by the desired product ($R_f = 0.46$). Yield: 0.42 g (31%). $^1$H NMR: 6.74 (s, 4H), 4.07 (quintet, 4H, $J$ = 7 Hz), 3.22 (m, 4H), 2.80 (s, 6H), 1.86−1.70 (m, 6H), 1.30 (t, 6H, $J$ = 6.5 Hz), 1.07 (t, 3H, $J$ = 7 Hz).

**Sodium 3-(Ethyl(*p*-(*N*,*N*-dimethylamino)phenyl)amino)-propyl-1-phosphonate (2).** Conversion of the diethylphosphonate to the free acid was carried out following Katz et al.:[17] diethyl 3-(ethyl(*p*-(*N*,*N*-dimethylamino)phenyl)amino)-propyl-1-phosphonate (0.42 g, 1.23 mmol) and bromotrimethylsilane (1.90 mL, 15 mmol) were dissolved in dry dichloromethane (10 mL) under Ar, and the resulting violet solution was stirred at r.t. for 15 h. The solvents and excess bromotrimethylsilane were removed by a Rotavapor under Ar. To the remaining brown gum was added a mixture of diethyl ether (10 mL), ethanol (10 mL), and collidine (1 mL), whereby a white solid was formed, which was filtered and washed with ether to afford 52 mg of **2**. The filtrate was concentrated to leave a paste that was washed with THF and acetonitrile to give another 120 mg white solid. The combined fractions were purified by dissolution in ethanol (5 mL), precipitation by addition of acetonitrile (50 mL), concentration to 20 mL, addition of more acetonitrile (30 mL), and so on, until no more precipitation occurred. Yield: 153 mg (44%) of 3-(ethyl(*p*-(*N*,*N*-dimethylamino)-phenyl)amino)propyl-1-phosphonic acid. $^1$H NMR ($CD_3OD$): 7.40 (d, 2H, $J$ = 9 Hz), 6.83 (d, 2H, $J$ = 9 Hz), 3.54−3.42 (m, 4H), 3.00 (s, 6H), 1.90−1.67 (m, 4H), 1.08 (t, 3H, $J$ = 7 Hz). Solutions of **2** were prepared by addition of 2 equiv of NaOH to the phosphonic acid in ethanol.

**Preparation and Characterization of the Nanocrystalline Layers.** In an argon glovebox, acetic acid (24.2 mL) was added to titanium isopropoxide (125 mL, Aldrich, 97%). This modified $TiO_2$ precursor was then added in one shot and at r.t., to deionized water (728 mL) under vigorous stirring. A white precipitate formed instantaneously, and the solution was left under stirring for 1 h to ensure completion of the hydrolysis and condensation reactions. Nitric acid (68%, 6 mL) was then added to bring the pH of the suspension to 1. The suspension was sonicated using a titanium ultrasonic horn from Bioblock Scientific Inc. and stirred for 2 h at 80 °C under reflux to achieve peptization (i.e., destruction of the agglomerates and redispersion into primary particles). The growth of these particles up to 20 nm was achieved under hydrothermal conditions in a titanium autoclave with a Teflon jacket heated for 12 h at 230 °C. Sedimentation took place during the autoclaving, and the particles were redispersed using an ultrasonic horn (400 W, 15 × 2 s pulses) and readjusting the pH to 1. After two sonications the colloidal suspension was concentrated in a Rotavapor (35 °C, 30 mbar) to a final $TiO_2$ concentration of 11 wt %. To prevent cracking during film drying, poly(ethylene glycol) (MW = 20 000, Merck) was added in a proportion of 50 wt % $TiO_2$. The resulting paste is stored in a screw-thread glass bottle until deposition.

The synthetic procedure for the preparation of the $ZrO_2$ colloids and films was similar. Zirconium *n*-propoxide (6 mL, 13.5 mmol, 70% in propanol) was mixed with acetic acid (0.775 mL, 13.5 mmol) under Ar. Under vigorous stirring, this mixture was added in one shot to $H_2O$ (25 mL) at r.t., resulting in the immediate formation of a colorless, jelly precipitate. After stirring for another 60 min, the propanol of the heterogeneous reaction mixture was distilled off in a Rotavapor. Then, $HNO_3$ (1 mL, 68%) was added, and the mixture was stirred at r.t. overnight for peptization. The peptized sol had the appearance of a homogeneous, transparent yellowish liquid. It was diluted with water to a total volume of 35 mL, transferred to a screw-capped Teflon container, and autoclaved at 230 °C for 12 h, which resulted in the formation of a stable, white colloid. The colloid was further processed as described for $TiO_2$ in order to obtain viscous, tape-castable pastes. Higher sol concentrations (15−17 wt %) were necessary though in order to obtain the appropriate viscosities.

$Al_2O_3$ colloïds were prepared as previously described.[18]

The colloidal pastes were deposited using a simple doctor blade technique on glass coated with conductive fluorine-doped $SnO_2$ (Nippon sheet glass, 8−10 ohms/square). The resulting layer was dried in air at r.t. for 10 min followed by 15 min at 50 °C. The film was then heated to 450 °C at 20−50°/min and left at 450 °C for 30 min before cooling to room temperature.

Treatment of the electrodes was effected as follows. To remove water and organic material adsorbed in the pores during storage, the electrodes were heated to 350 °C for 30 min in an air stream. Derivatization was done by immersing the still hot (100 °C) electrode in a submillimolar solution of the derivatizing agent in absolute ethanol. After 12 h at r.t., the electrodes were rinsed with absolute ethanol, dried briefly (1 min) at 100 °C, and used directly or stored in cyclohexane.

## Results

**Structure of the Nanocrystalline Layers.** The specific surface area of the $TiO_2$ nanocrystalline electrodes was found to be 91 $m^2/g$, which gives a crystallite size around 17 nm, assuming the particles are quasi-spherical. This was confirmed by scanning electron microscopy (Figure 1). The pore size distribution (Figure 1) is centered around 20 nm. X-ray diffraction analysis showed that the particles are composed of anatase (no rutile detected), and transmission electron micrography revealed that the main orientation of the lattice planes at the particle surface is (101). For $ZrO_2$, XRD analysis showed that the powder consists of the thermodynamically stable

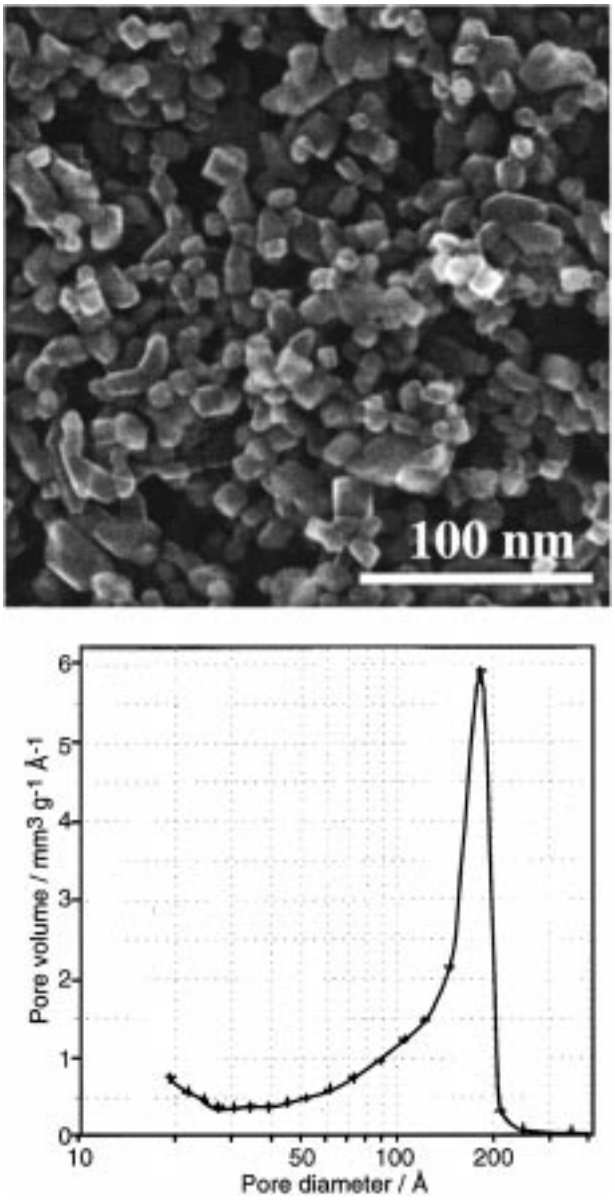


**Figure 1.** Top: scanning electron micrograph of a nanocrystalline $TiO_2$ film. Bottom: pore size distribution in a nanocrystalline $TiO_2$ film as determined by nitrogen adsorption, using the BET formalism.

monoclinic crystal modification (baddeleyite) with no detectable amounts of any of the other crystal phases. The specific surface area of the powders is 121 $m^2/g$ as determined by nitrogen adsorption on a Gemini 2375 apparatus (Micromeretics) using the BET formalism. This corresponds to an average particle diameter of about 8.5 nm, assuming spherical, monodispersed particles with the density of baddeleyite (5.89 $g/cm^3$).

The roughness factor $\eta$ of the electrodes, defined as the ratio of the effective surface area of the nanocrystalline layer to its projected area, was determined by derivatization with a phosphonated dye. The ruthenium complex (4,4′,4″-$Me_3$terpy)Ru(terpy-$PO_3H$) (**4**) was used, where 4,4′,4″-$Me_3$terpy is 4,4′,4″-trimethyl-2,2′:6′,2″-terpyridine and terpy-$PO_3H$ is 2,2′:6′,2″-terpyridine-4′-hydrogenophosphonate. The diameter of the molecule (16 Å), determined by molecular modeling, is close to the diameter of **1**, as measured between the two methoxy groups. On can thus assume that both molecules will be able to penetrate more than 90% of the pores, based on the size distribution shown in Figure 1. The absorbance $A$ of a nanocrystalline layer bearing a monolayer of molecules characterized by an extinction coefficient $\epsilon$ and a molecular surface $S_{mol}$ is given by eq 2.

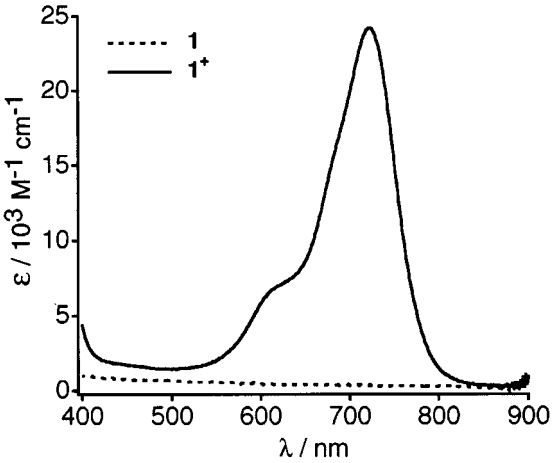


**Figure 2.** Visible absorption spectra of **1** (---) and $\mathbf{1}^+$ (—) in acetonitrile/THF (4:1). Oxidation of **1** to $\mathbf{1}^+$ was done in a photoelectrochemical cell, on carbon felt, increasing the potential stepwise from 0.7 to 1.2 V, allowing for spectrum stabilization between steps. Absorption maximum was reached at 1.0 V.

$$A = \eta\epsilon/(N_A S_{mol}) \quad (2)$$

The absence of aggregation of the dye on the surface is of course a prerequisite for proper roughness determination. The complex **4** fulfills that condition. Its $\epsilon$ is 15 300 $M^{-1}$ $cm^{-1}$ at 482 nm, and $S_{mol}$ was calculated to be 200 $Å^2$. The absorbance at that wavelength of the $TiO_2$ electrodes derivatized with **4** was $A = 0.80 \pm 0.05$, yielding a roughness factor equal to 630 $\pm$ 40. For the $Al_2O_3$ electrodes, we obtained a value of 520 $\pm$ 40.

**Adsorption Behavior.** The adsorption isotherms of **1** were established by derivatizing electrodes from solutions of different concentrations, oxidizing the adsorbed molecules chemically by $NOBF_4$, and measuring the absorbance of the electrodes at 750 nm, where $\epsilon$ of $\mathbf{1}^+$ is 15 200 $M^{-1}$ $cm^{-1}$ (see Figure 2). That wavelength was preferred to the absorption maximum ($\lambda_{max}$ = 730 nm, $\epsilon$ = 24 000 $M^{-1}$ $cm^{-1}$) in order avoid too high absorbance values. The surface concentrations $\Gamma$ were obtained by eq 3.

$$\Gamma = A/(\eta\epsilon) \quad (3)$$

The experimental values were fitted to a Langmuir adsorption isotherm (Figure 3), as expressed by eq 4,

$$\Gamma = \Gamma^\circ C/(C + 1/K) \quad (4)$$

where $C$ is the concentration in solution, $\Gamma^\circ$ is the surface concentration in the saturated monolayer, and $K$ is the adsorption constant. The best fit for $TiO_2$ was obtained with $\Gamma^\circ = 3.3 \pm 0.1$ $\mu$mol/$m^2$ and $K$ = 26 000 $\pm$ 2000 $M^{-1}$. For $Al_2O_3$, the respective values were 2.9 $\pm$ 0.1 $\mu$mol/$m^2$ and 33 000 $\pm$ 4000 $M^{-1}$.

The adsorption constant of **1** on $TiO_2$ is close to that obtained for the phosphonated viologen **3** ($K$ = 24 000 $M^{-1}$).[19]

$$S_{mol} = 1/(\Gamma^\circ N_A) \quad (5)$$

**Electrochemistry.** The radical cations of trianisylamine and *N*,*N*,*N*′,*N*′-tetraalkyl-*p*-phenylenediamines as well as the radical anions of viologens are known to be fairly stable in solution.[20] As expected, the corresponding phosphonated molecules **1**, **2**,

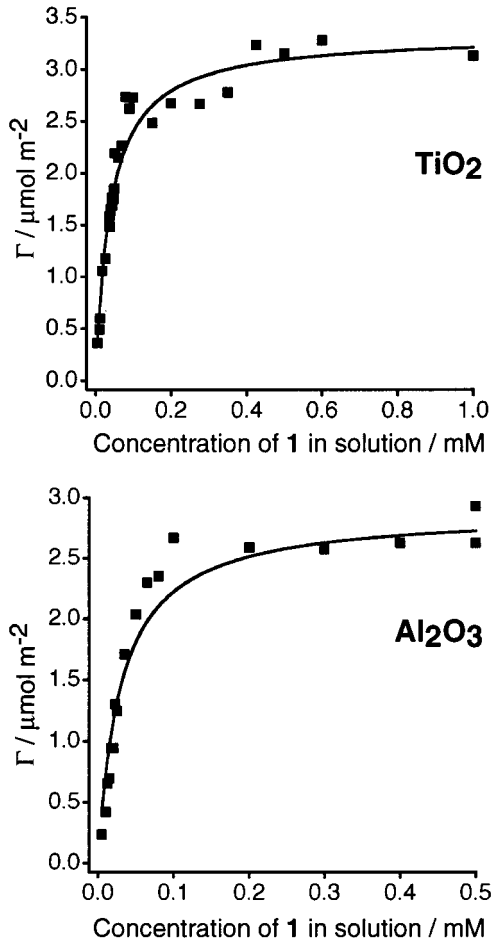


**Figure 3.** Adsorption isotherms of **1** on nanocrystalline $TiO_2$ and $Al_2O_3$ layers from ethanolic solutions: measured points (squares) and best fit of the Langmuir equation (line).

and **3** displayed reversible electrochemical behavior in acetonitrile or propylene carbonate, with the redox potentials given in the Introduction. The situation was different in the adsorbed state. Nanocrystalline $TiO_2$ electrodes derivatized with **1**, **2**, and **3** were submitted to cyclic voltammetry in propylene carbonate. The recorded traces, presented in Figure 4a, clearly show the particular behavior of the triarylamine **1**. Integration of the oxidation wave of **1** gave 13.2 mC, corresponding to $\Gamma^\circ = 2.3$ $\mu$mol/m$^2$, but only 7.53 mC for the reduction wave, denoting probably a partial desorption of $\mathbf{1}^+$ in the polar solvent used. In the ambient temperature molten salt 1-ethyl-3-methylimidazolium bis(trifluoromethylsulfonyl)imide ($EtMeIm^+Tf_2N^-$, specific conductivity 8.8 mS cm$^{-1}$)[21] oxidation and reduction charges were equal. This medium was chosen for further electrochemical investigations as it grants a satisfactory long-term stability to the monolayer, as shown by the absence of noticeable degradation established during 100 voltammetric cycles. In acetonitrile containing lithium salt, the system exhibited also a completely reversible behavior (Figure 4b). Observations were similar on nanocrystalline $ZrO_2$ films (Figure 4c).

The adsorbed *p*-phenylenediamine **2** underwent a slow oxidation at 0.5 V, but the reduction only occurred below −0.3 V. The viologen **3** behaved completely irreversibly. Its reduction took place only when electrons were injected from the conduction band of the $TiO_2$, but no oxidation wave was observed, these electrons being trapped in the reduced viologen, below the conduction band edge. Reversibility was obtained

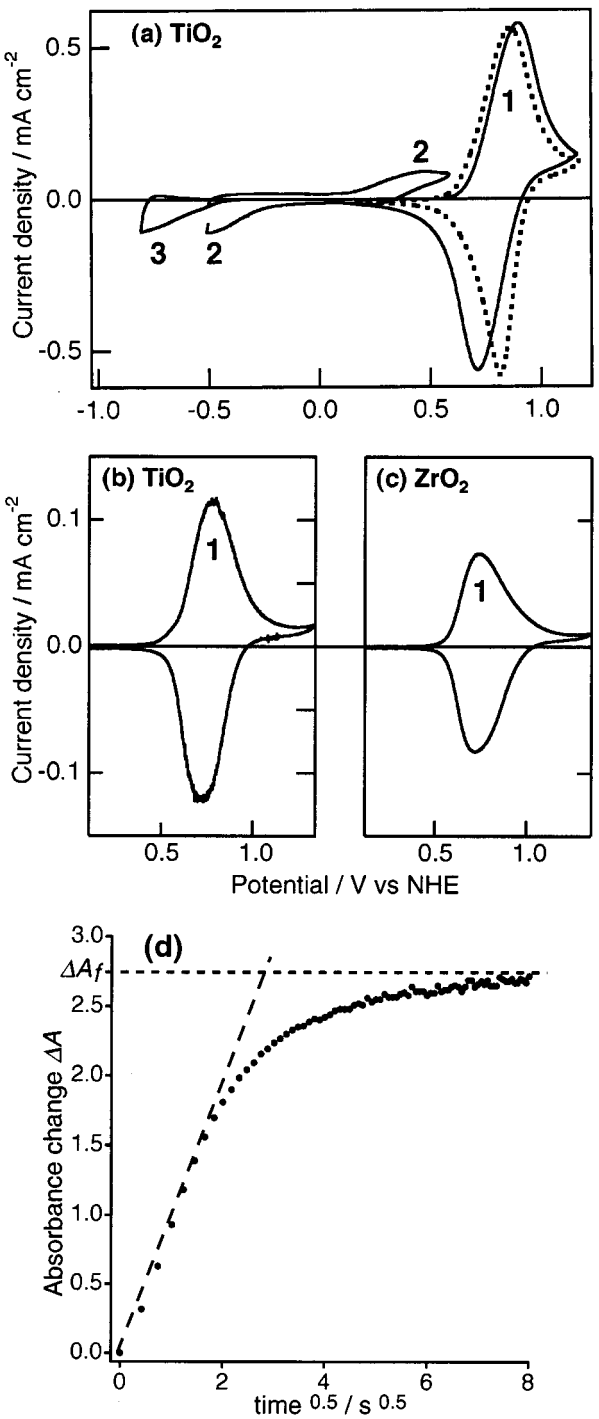


**Figure 4.** Cyclic voltammograms of nanocrystalline electrodes derivatized by **1**, **2**, and **3**: (a) in propylene carbonate + 0.2 M $NBu_4^+TfO^-$ at (—) 20 mV/s and (---) 2 mV/s with vertical expansion 7×; (b) and (c) in acetonitrile + 0.5 M $Li^+Tf_2N^-$ at 2 mV/s. (d) Optical Anson plot for nanocrystalline $TiO_2$ electrodes derivatized with **1**, in $EtMeIm^+Tf_2N^-$. The absorbance $A$ was recorded as a function of the square root of time, following a potential step from 0.2 to 1.0 V. Linearity is observed over 60% of the oxidation process, following what $A$ tends asymptotically toward $A_f = 2.7$.

in the presence of lithium ions, the latter lowering the conduction band edge below the redox potential of the viologen.[3]

The electrodes derivatized with **1** displayed striking electrochromism. Typically, their aspect turned from colorless to deep blue ($\Delta A > 2$ between 730 and 770 nm) when the applied potential changed from 0 to 1 V or more. In polar, highly conductive solvents such as acetonitrile, propylene carbonate,

or 3-methoxypropionitrile, the process was very fast: coloration or discoloration occurred in less than 2 s following a potential step up from 0.2 to 1.0 V or down from 1.0 to −0.15 V, respectively. For practical electrochromic applications that require long-term stability, $EtMeIm^+Tf_2N^-$ appears better suited despite the longer switching time ($\Delta A = 1.5$ in 7 s, $\Delta A = 2$ in 30 s).

The apparent diffusion coefficients were measured at different surface concentrations of **1**, using a chronospectrophotometric method derived from the classical chronocoulometric method.[22] Following a potential step, the charge $Q$ exchanged with a modified electrode evolves with time following eq 6, where $S$ is the electrode surface area and $C$ is the concentration of the electroactive species in the film. $C$ can be obtained via eq 7, from the film thickness $d$ and the total charge $Q_f$ necessary to obtain full redox change of the electroactive centers. Substitution affords eq 8. As this model describes a semiinfinite diffusion phenomenon, it holds only as long as the oxidative or reductive front has not reached the limit of the electroactive layer. Hence, in an Anson plot ($Q$ versus $t^{0.5}$), the first part is linear, according to eq 6, followed by a curved region in which $Q$ asymptotically tends toward $Q_f$.

$$Q = 2nFSCD_{app}{}^{0.5}t^{0.5}/\pi^{0.5} \quad (6)$$

$$C = Q_f/nFSd \quad (7)$$

$$Q = 2Q_fD_{app}{}^{0.5}t^{0.5}/(d\pi^{0.5}) \quad (8)$$

In the case of an electrochromic film, where the absorbance change $\Delta A$ is proportional to the charge passed, eqs 6 and 8 can be transformed into the corresponding eqs 9 and 10. Optical equivalents of Anson plots are obtained by measuring $\Delta A$ versus $t^{0.5}$. Compared to chronocoulometry, chronospectrophotometry ensures that only the redox phenomena involving the studied species are recorded. Figure 4d shows a typical optical Anson plot. The linearity observed for the first half of the absorption change supports the diffusion control of the process. The highest apparent diffusion coefficients recorded on $TiO_2$ in $EtMeIm^+Tf_2N^-$ were $2.8 \times 10^{-12}$ m$^2$ s$^{-1}$.

$$\Delta A = 2C\epsilon D_{app}{}^{0.5}t^{0.5}/\pi^{0.5} \quad (9)$$

$$\Delta A = 2\Delta A_fD_{app}{}^{0.5}t^{0.5}/(d\pi^{0.5}) \quad (10)$$

To discriminate between a charge transport by molecular diffusion to the conducting glass and a charge transport by electron hopping, the apparent diffusion coefficient was measured as a function of the surface concentration of the electroactive molecule **1**. This surface concentration was controlled in two ways: in a first series of experiments by coadsorbing a nonelectroactive molecule and in a second one by varying the concentration of **1** in solution, in the submonolayer domain of the Langmuir isotherm.

For the experiment involving a redox-inert coadsorbent, compound **5** was used as a surface diluant. As it is composed, like **1**, of an aromatic head and of a propylphosphonate tail, it was supposed to form with **1** homogeneous mixed monolayers of a similar structure as the pure monolayer. The apparent diffusion coefficient is plotted in Figure 5a as a function of the molar fraction $x_1$ of **1** in a solution of **1** and **5**. The total concentration of the two species was always 0.50 mM. The molar fraction in the monolayer was measured to be the same[23] as in the derivatizing solution. Clearly, $D_{app}$ varies with $x_1$, with a percolation threshold around $x_1 = 0.5$.

For the experiment of surface dilution without coadsorbent, $TiO_2$ electrodes were derivatized with 0.005−1 mM solutions of **1**. The surface concentrations were determined as for the Langmuir isotherm and ranged from 0.35 to 3.3 $\mu$mol/m$^2$. Figure 5b shows the variation of $D_{app}$ with the surface concentration. Here again, it is clear that $D_{app}$ varies with $\Gamma$, above a percolation limit situated around 1.7 $\mu$mol/m$^2$, corresponding, to 50% of a full monolayer. The fraction of **1** that was electrochemically oxidizable is plotted in Figure 5d as a function of the surface concentration. The measure was taken 340 s after the potential step, a delay during which an absorbance plateau was reached in all the cases. The percolation threshold is particularly striking in this type of representation. Below 1.7 $\mu$mol/m$^2$, almost no molecules of **1** can be oxidized electrochemically. Above that limit, all the molecules are accessible.

On $Al_2O_3$, similar behavior was observed (Figure 5c). The wider points distribution and the lower apparent diffusion coefficients can be attributed to a worse adherence of the nanocrystalline layer on the conducting glass.

To investigate the correlation between the apparent diffusion coefficient and the properties of the contacting medium, $D_{app}$ was recorded in a series of blends of $EtMeIm^+Tf_2N^-$ with various solvents. The values obtained for a full monolayer of **1** with different compositions of a $EtMeIm^+Tf_2N^-$−methoxypropionitrile (MPN) mixture are reported in Figure 6a. $D_{app}$ increases rapidly between 1% and 25% of $EtMeIm^+Tf_2N^-$ and then decreases for higher salt concentrations. Comparison of the apparent diffusion coefficient measured in 1:1 mixtures of $EtMeIm^+Tf_2N^-$ with solvents of different dielectric constants is presented in Table 1. In Figure 6b, the apparent diffusion coefficients measured in $EtMeIm^+Tf_2N^-$−MPN (1:1) at various surface concentrations are compared with the values obtained in the neat liquid salt. Clearly, $D_{app}$ is higher in the blend than in the pure salt, at any concentration above the percolation threshold.

## Discussion

The average surface occupied by each molecule of **1** in the saturated monolayer was calculated by eq 5 to be $S_{mol} = 50 \pm 2$ Å$^2$. That area is particularly small. In fact, if the molecule would lie horizontally on the $TiO_2$ or if, while perpendicular to the surface, the triarylamine moiety would be freely rotating, the molecule would occupy at least 200 Å$^2$. The much smaller value obtained for $S_{mol}$ indicates a high degree of self-assembly in the monolayer. If we consider the planar triarylamine moieties as perpendicular to the surface, with a projected methyl−methyl distance of 13−16 Å, depending on the position of these groups, then the interplanar distance should be 3−4 Å (see Figure 8a), which indeed corresponds to a full stacking of the molecules.

Both the dependence of the apparent diffusion coefficient on the surface concentration and the existence of a percolation limit for the conductivity of the monolayers of **1** indicate that the charge motion takes place by hopping and not by molecular diffusion, as depicted in Figure 8. The percolation threshold ($p_c$) for the conductivity inside a composite material corresponds to a critical concentration above which an infinite cluster of conductive sites spans the network. $p_c$ is dependent on both the dimensionality and the coordination number $Z$ of the lattice.[24] The observed percolation threshold, at $x_1 = 0.5$ or $\Gamma = 0.5\Gamma^\circ$, is consistent with a two-dimensional triangular ($Z = 6$) or square ($Z = 4$) lattice in the *site percolation* model. The calculated

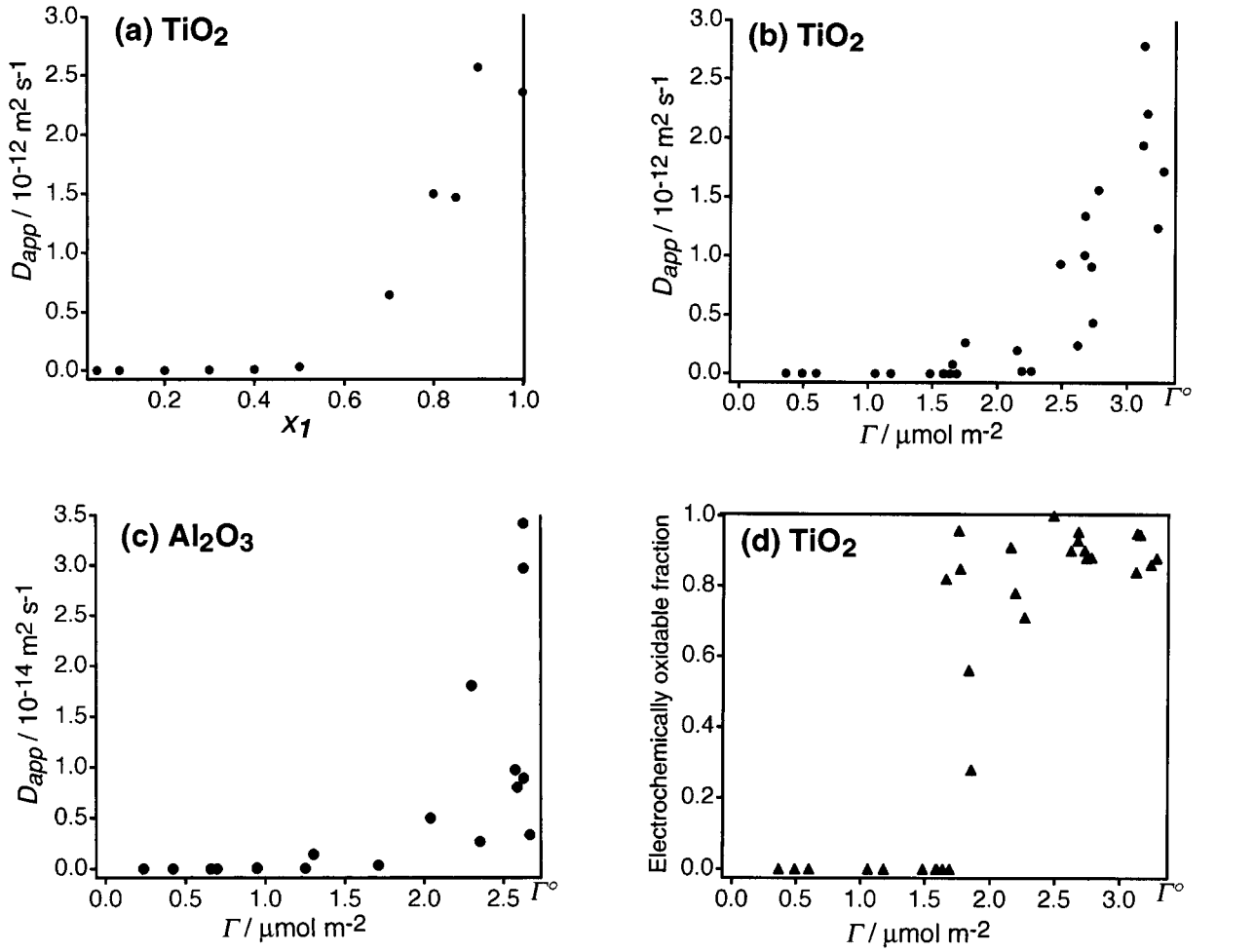


**Figure 5.** $D_{app}$ for the oxidation of a monolayer of **1** on nanocrystalline films, in $EtMeIm^+Tf_2N^-$, following a potential step from 0.2 to 1.0 V: (a) as a function of the molar fraction of **1** ($x_1$) in a mixed monolayer of **1** and **5** on $TiO_2$; (b) as a function of the surface concentrations of **1**, in the absence of coadsorbent, on $TiO_2$; (c) idem on $Al_2O_3$. (d) Electrochemically oxidizable fraction of a monolayer of **1** on a $TiO_2$ nanocrystalline film, measured at different surface concentrations of **1**, after 340 s at a potential of 1.0 V.

values for these types of lattices are $p_c = 0.5$ and $p_c = 0.59$, respectively. Those lattices correspond to an electron hopping possible between each molecule and its four to six closest neighbors, as illustrated in Figure 8b.

In the model of Blauch and Savéant,[9b] the percolation behavior was analyzed as a function of the spatial extension of the electronic coupling characterizing the hopping process. The classical exponential decrease of the electron-transfer rate constant $k_{ex}(r)$ with the intermolecular distance $r$ was considered, according to eq 11, in which $k°_{ex}$ is the rate at the closest distance $\delta$, and $\gamma$ is the damping parameter of the electron transfer.

$$k_{ex}(r) = k°_{ex} e^{-(r-\delta)/\gamma} \qquad (11)$$

In a classical percolation case, the electron hopping occurs only between adjacent sites ($\gamma = 0$) and $D_{app} = 0$ below the critical fractional loading $p_c$. For $\gamma > 0$, electrons can hop across distances larger than $\delta$ and can hence escape from an isolated cluster, thereby allowing some conductivity of the material below the percolation threshold. We observed in fact a nonzero value of $D_{app}$ below $x_1 = 0.5$ (or below $\Gamma = 0.5\Gamma°$). In Figure 7, the observed $D_{app}$ versus $x_1$ variation is compared with the predictions of the model for different values of $\gamma/\delta$ in a square lattice. On the basis of that comparison, we attribute to our system a value $\gamma/\delta = 0.13 \pm 0.05$. Assuming $\delta = 4$ Å, we get $\gamma = 0.52 \pm 0.20$ Å, which is not far from values reported for electron transfers between aromatic molecules in rigid glasses ($\gamma = 0.58-0.83$ Å).[25] This fast damping means that the electron hopping does not extend significantly beyond the next neighbor.

The structure and electrochemical properties of the adsorbed molecules seem essential for the appearance of an efficient lateral charge transport. The reason electron hopping is efficient in monolayers of **1** is very likely related to the high self-exchange rate of these amines. Viologens or electrochemically reversible ruthenium complexes grafted on nanocrystalline layers do not display lateral charge percolation, at least not to a comparable extent.[26] Self-exchange rate constants in acetonitrile were reported to be $8.4 \times 10^6$ $M^{-1}$ $s^{-1}$ for dimethyl viologen$^{2+/+}$,[27] $3.5 \times 10^7$ $M^{-1}$ $s^{-1}$ for $Ru(Me_2bipy)(hfac)_2$ ($Me_2$-bipy = 4,4′-dimethyl-2,2′-bipyridine, hfac = hexafluoroacetylacetonate),[28] and $(5.3-7.7) \times 10^9$ $M^{-1}$ $s^{-1}$ for *N,N,N′,N′*-tetramethyl-*p*-phenylenediamine$^{+/0}$.[29] The latter value is close to the diffusion-limited rate constant $k_D = 2.1 \times 10^{10}$ $M^{-1}$ $s^{-1}$. We assume that for triarylamines the self-exchange rate constant is of the same order of magnitude as for *p*-phenylenediamines. Hence, as the conductivity in a monolayer of **2** is much lower than in a monolayer of **1**, it seems that a fast electron self-exchange in solution is a necessary but not sufficient condition for efficient lateral charge motion. The fast charge percolation inside monolayers of **1** must thus be attributed to the almost planar geometry of the molecules, which allows compact

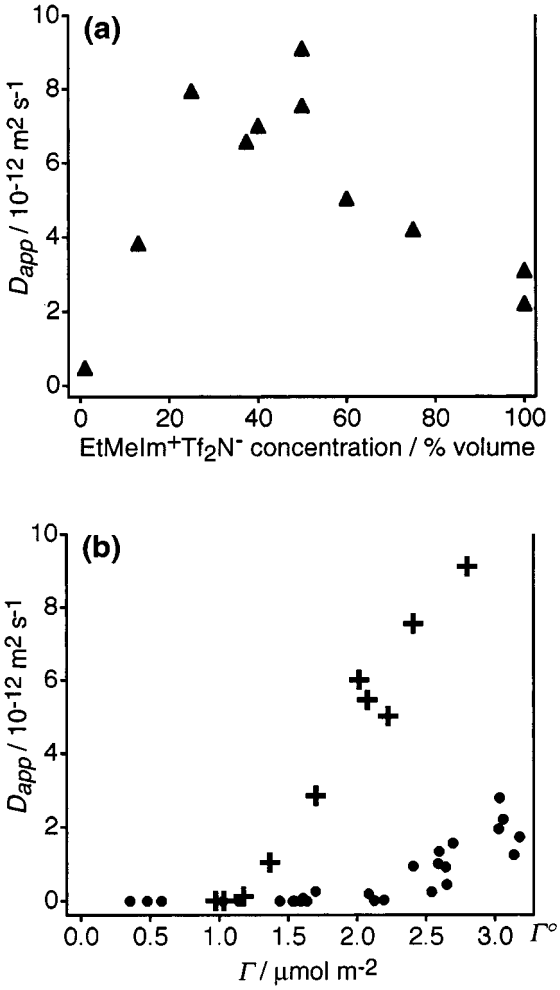


**Figure 6.** $D_{app}$ for the oxidation of a monolayer of **1** on nanocrystalline $TiO_2$ films (a) in different methoxypropionitrile−$EtMeIm^+Tf_2N^-$ blends between 99:1 and 0:100 ratios by volume and (b) as a function of the surface concentration of **1**, in 1:1 methoxypropionitrile−$EtMeIm^+Tf_2N^-$ (+) and in neat $EtMeIm^+Tf_2N^-$ (●).

**TABLE 1: Apparent Diffusion Coefficients in a Full Monolayer of 1 on $TiO_2$, in Different $EtMeIm^+Tf_2N^-$−Solvent (1:1) Blends**

| nanocrystalline material | solvent | $\epsilon^b$ | $D_{app}{}^c/10^{-12}$ $m^2\,s^{-1}$ |
|---|---|---|---|
| $TiO_2$ | diglyme[a] | 7 | 2.6 |
| $TiO_2$ | $EtMeIm^+Tf_2N^-$ | ⩽10 | 2.8 |
| $TiO_2$ | 4-methyl-2-pentanone | 13 | 5.0 |
| $TiO_2$ | 3-methoxypropionitrile | 20 | 9.1 |
| $TiO_2$ | acetonitrile | 37 | 11 |
| $Al_2O_3$ | $EtMeIm^+Tf_2N^-$ | ⩽10 | 0.035 |
| $ZrO_2$ | acetonitrile | 37 | 4.6 |

[a] Diethylene glycol dimethyl ether. $EtMeIm^+Tf_2N^-$ is not miscible with solvents of dielectric constant lower than 7. [b] Dielectric constant of the solvent. [c] Highest measured values are given, assumed to correspond to the best nanocrystalline films. Estimated error 10%.

stacking perpendicular to the metal oxide surface and thus probably a high degree of self-organization in the monolayer.

The physical meaning of the apparent diffusion coefficient in our system can be equivocal and deserves to be discussed. During the oxidation or reduction of the adsorbed monolayer, electrons hop from molecule to molecule while ions move at the monolayer boundary to compensate the charge variation and further flow through the pores of the metal oxide. Thus, the apparent diffusion coefficient can reflect the motion of either

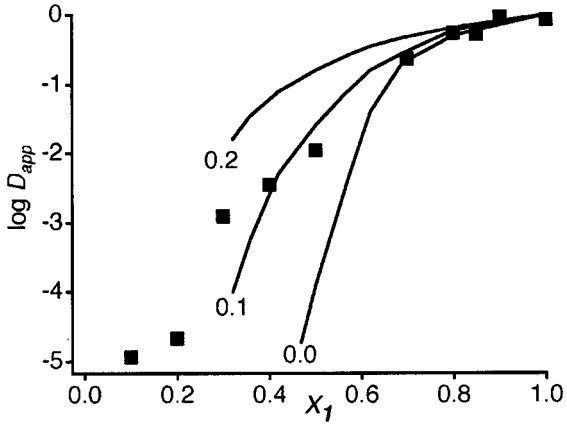


**Figure 7.** Variation of $\log(D_{app})$ (■) with the molar fraction of **1** ($x_1$) in a mixed monolayer of **1** and **5** on $TiO_2$ compared with the simulations of Blauch and Savéant[9b] (lines with indicated value of $\gamma/\delta$).

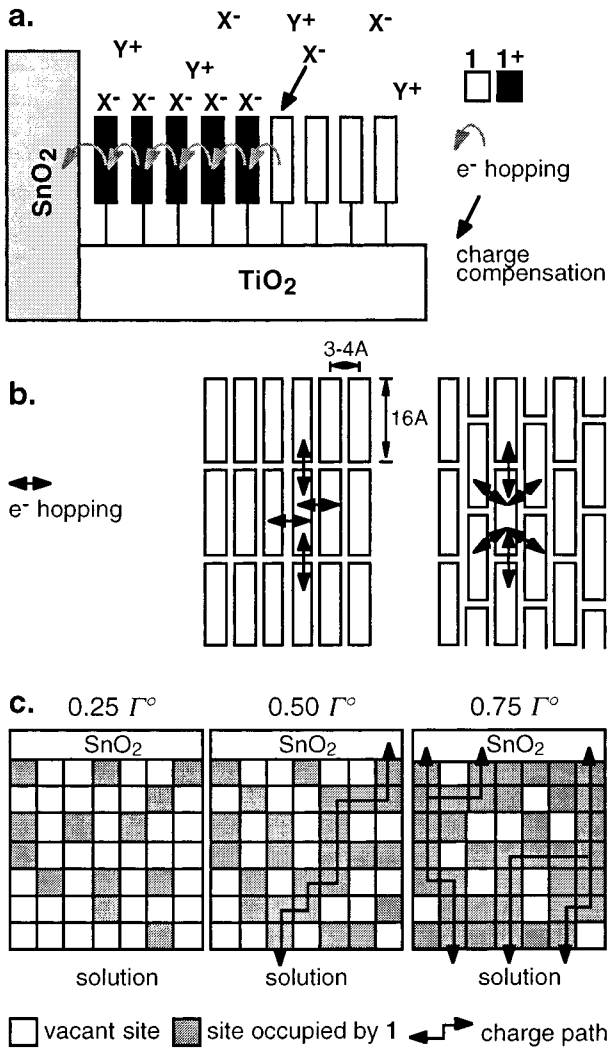


**Figure 8.** Proposed mechanism for a lateral charge transport inside a monolayer of amines **1** on porous metal oxide on conductive substrate: (a) cross section of a half pore; (b) top view of a monolayer with possibilities of electron hopping in a square (left) and in a triangular (right) lattice; (c) scheme of a metal oxide surface bearing various submonolayer surface concentrations of **1** in a square lattice, with charge paths opening above the percolation threshold ($\Gamma \geqslant 0.5\Gamma°$).

the electrons or the ions or a combination of both. From the observation that the apparent diffusion coefficient strongly depends on the surface concentration of the electroactive molecules, one can infer that the resistance of the electrolyte in

the pores was never limiting in our experiments. In fact, if the ion motion in the pores would be the slowest process, one would expect that the apparent diffusion coefficient would remain independent of the surface concentration over a range comprised between the full coverage and a value at which the electron hopping process would become the rate limiting process. This is obviously not the case, as $D_{app}$ continuously varies with $\Gamma$ above the percolation threshold. Hence, we conclude that the conductivity of the solutions was high enough to avoid current limitation by bulk resistance of that medium. However, it appears clearly from the entire Figure 6 that the apparent diffusion coefficient is not only controlled by the surface concentration of the amine **1** but also depends strongly on the nature of the contacting medium. Diluting the liquid salt by a polar solvent leads to an increase of $D_{app}$. What is the relevant parameter? Both the viscosity[31] and the dielectric constant[32] of the medium are known to influence the rate of an intermolecular electron transfer in solution. As the proportion of liquid salt diminishes, the viscosity decreases while, with polar solvents, the dielectric constant increases. It was in fact shown that at the molecular level $EtMeIm^+Tf_2N^-$ behaves like a solvent of low dielectric constant ($\epsilon \leq 10$).[21] In the present case, solvent molecules are not supposed to be present between the closely packed electroactive molecules of the monolayer, and thus, the viscosity is not expected to affect the rate of electron transfer. Consistently, similar values of $D_{app}$ were obtained in $EtMeIm^+$-$Tf_2N^-$−diglyme blends and in the pure liquid salt despite very different viscosities (5.3 and 34 cP, respectively). The dielectric constant, on the contrary, does affect the charge-transfer rate via the solvent reorganization energy which makes an important contribution to the total activation energy of the process, even when there are no solvent molecules between an electron donor and an electron acceptor, like in intramolecular electron transfers. However, the observed effect is opposite to the expectation: the solvent reorganization energy increases with $\epsilon$, and thus, the electron-transfer rate should decrease, as formalized in the Marcus theory.[32] We observed, on the contrary, that $D_{app}$ increases with $\epsilon$. The only way to deal with these apparent contradictions is to postulate that the overall charge percolation process, measured by $D_{app}$, is comprised of more than one elementary process. At the molecular level, each molecule is oxidized or reduced by electron transfer to its neighbor. That first process is probably the fastest and, hence, not rate limiting. At the same time, charge compensation must take place by ion motion at the monolayer boundary. In the pure $EtMeIm^+Tf_2N^-$ or blends with low-$\epsilon$ solvents, ion pairing is strong, and hence, the process is slow because pairs need to be dissociated to afford free ions. With a solvent of high dielectric constant added, ion pairs are separated, which allows faster ion motion for charge compensation, leading to higher values of $D_{app}$. If however the ion concentration decreases too much (below ca. 1 M in MPN), the advantage of dissociating the ion pairs is overcompensated by the longer average diffusion distance to cross for the ion closest to the monolayer. As a result, $D_{app}$ drops, the curved region of the Anson plot progressively vanishes, and the absorbance of the electrode ultimately grows linearly with the square root of the time, up to $A_f$. The whole process of space charge compensation is obviously rate limiting. The third factor controlling $D_{app}$ is charge percolation at the mesoscopic oxide surface. The individual electron-transfer step being limited by charge compensation, we can assume that it takes place at the same rate for every molecule pair at any surface concentration of **1** above the percolation limit. As a consequence, the origin of the effect of surface concentration on $D_{app}$ is not molecular but very likely reflects only the density of conducting paths on the surface. In fact, there cannot be two rate-limiting processes at the molecular level. If we postulate that charge compensation limits the intermolecular electron hopping rate, we must admit that the surface concentration does not restrict it under the same conditions. However, as both the dielectric constant and the surface concentration affect $D_{app}$ simultaneously, the control by the latter parameter must take place at a superior scale: the mesoscopic architecture of the entire monolayer where the complexity and thus the length of the way a charge has to follow to reach the electrode depends on the density of open paths. One can formalize this model by eq 12. It is in that way possible to account for the existence of two limiting processes affecting the apparent diffusion coefficient simultaneously.

$$D_{app} \sim \text{rate of electron transfer} \times \text{density of conducting paths} \quad (12)$$

The apparent rate constant $k_{ex}$ for the bimolecular electron-transfer process can be obtained via eq 13,

$$k_{ex} = 6D_{app}d\epsilon/(\delta^2 \Delta A_f) \quad (13)$$

derived from eq 1, which is assumed to be valid at full fractional loading ($\Gamma = \Gamma^\circ$), by substituting the concentration by $\Delta A_f/\epsilon d$. With $D_{app} = 2.8 \times 10^{-12}$ m$^2$ s$^{-1}$ in $EtMeIm^+Tf_2N^-$ and 2 Å < $\delta$ < 4 Å, we get $10^6$ M$^{-1}$ s$^{-1}$> $k_{ex}$ > $3 \times 10^5$ M$^{-1}$ s$^{-1}$. The theoretical diffusion-limited rate constant ($k_D$) in this medium is $10^7$ M$^{-1}$ s$^{-1}$, according to the Smolukovsky−Debye relationship.[30] $k_{ex}$ is 1 order of magnitude lower than $k_D$, which is consistent with a rate limitation imposed by charge compensation. The rate of the pure electron hopping step is probably much higher as it does not imply any diffusion process. This value could be obtained in a steady-state conductivity measurement, with a nanocrystalline $TiO_2$ film derivatized with **1** deposited on a microelectrodes array.[33] This work is in progress.

**Conclusions**. The self-organized monolayer of a phosphonated triarylamine anchored on a nanocrystalline metal oxide behaves like an electronically conducting polymer, as illustrated by the dependence of the apparent diffusion coefficient on the concentration of the electroactive species and by the existence of a percolation threshold for the conductivity of the assembly. The possibility of lateral charge transport at the surface of nanocrystalline semiconductor layers further broadens the field of their applications. Not only species having redox levels in the vicinity of the conduction band of the material can be electroactive but also species prone to fast electron hopping and able to form compact self-organized monolayers, in which case the nanocrystalline semiconductor only acts as an inert supporting material exploited for its high surface area. This opens the way to new electrochromic, electrocatalytic, and sensor applications.

**Acknowledgment.** This work was supported by the Swiss National Science Foundation (FNRS) and (for S.T.) by the European TMR program. The authors are grateful to Dr. A. J. McEvoy for useful discussions.

### References and Notes

(1) Gerfin, T.; Grätzel, M.; Walder, L. *Prog. Inorg. Chem.* **1997**, *44*, 345−393.

(2) (a) O'Reagan, B.; Grätzel, M. *Nature* **1991**, *353*, 737−739. (b) Nazeeruddin, M. K.; Kay, A.; Rodicio, J.; Humphrey-Baker, R.; Müller, E.; Liska, P.; Vlachopoulos, N.; Grätzel, M. *J. Am. Chem. Soc.* **1993**, *115*,

6382−6390. (c) Nazeeruddin, M. K.; Liska, P.; Vlachopoulos, N.; Grätzel, M. *Helv. Chim. Acta* **1990**, *73*, 1788−1803.

(3) (a) Hagfeldt, A.; Vlachopoulos, N.; Gilbert, S.; Grätzel, M. *Proc. SPIE−Int. Soc. Opt. Eng. XIII* **1994**, *2255*, 297−304. (b) Hagfeldt, A.; Walder, L.; Grätzel, M. *Proc. SPIE−Int. Soc. Opt. Eng. XIV* **1995**, *2531*, 60−69. (c) Campus, F.; Bonhôte, P.; Grätzel, M.; Heinen, S.; Walder, L. *Sol. Energy Mater.*, in press.

(4) Shinohara, H.; Grätzel, M.; Vlachopoulos, N.; Aizawa, M. *Bioelectrochem. Bioenerg.* **1991**, *26*, 307−320.

(5) Mayor, M.; Hagfeldt, A.; Grätzel, M.; Walder, L. *Chimia* **1996**, *50*, 47−49.

(6) Bonhôte, P.; Moser, J. E.; Vlachopoulos, N.; Walder, L.; Zakeeruddin, S. M.; Humphry-Baker, R.; Péchy, P.; Grätzel, M. *J. Chem. Soc., Chem. Commun.* **1996**, 1163−1164.

(7) Finklea, H. O., Ed. *Semiconductor Electrodes*; Elsevier: Amsterdam, 1988; pp 108−114.

(8) Majda, M. In *Molecular Design of Electrode Surfaces*; Murray, J., Ed.; Wiley-Interscience: New York, 1992; Chapter IV, pp 159−184.

(9) (a) Blauch, D. N.; Savéant, J.-M. *J. Am. Chem. Soc.* **1992**, *114*, 3323−3332. (b) Blauch, D. N.; Savéant, J.-M. *J. Phys. Chem.* **1993**, *97*, 6444−6448.

(10) See note 10 in ref 9b.

(11) (a) Dahms, H. *J. Phys. Chem.* **1968**, *72*, 362−365. (b) Ruff, I.; Friedrich, V. J. *J. Phys. Chem.* **1971**, *75*, 3297−3302. (c) Ruff, I.; Friedrich, V.; Demeter, K.; Csaillag, K. *J. Phys. Chem.* **1971**, *75*, 3303−3309.

(12) (a) Laviron, E. *J. Electroanal. Chem.* **1980**, *112*, 1−9. (b) Andrieux, C. P.; Savéant, J.-M. *J. Electroanal. Chem.* **1980**, *111*, 377−381. (c) Anson, F. C.; Blauch, D. N.; Savéant, J.-M.; Shu, C. F. *J. Am. Chem. Soc.* **1991**, *113*, 1922−1932. (d) Fritsch-Faules, I.; Faulkner, L. R. *J. Electroanal. Chem.* **1989**, *263*, 237−255.

(13) Miller, C. J.; Majda, M. *J. Electroanal. Chem.* **1986**, *207*, 49−72.

(14) (a) Miller, C. J.; Majda, M. *J. Am. Chem. Soc.* **1986**, *108*, 3118−3120. (b) Miller, C. J.; Widrig, C. A.; Charych, D. H.; Majda, M. *J. Phys. Chem.* **1988**, *92*, 1928−1936. (c) Miller, C. J.; Majda, M. *J. Phys. Chem.* **1988**, *92*, 2, 1937−1942.

(15) Shigehara, K.; Oyama, N.; Anson, F. C. *J. Am. Chem. Soc*. **1981**, *103*, 2552−2558.

(16) (a) Majda, M. *Thin Films* **1995**, *20*, 331−347. (b) Charych, D. H.; Anvar, D. J.; Majda, M. *Thin Solid Films* **1994**, *242*, 1.

(17) Katz, H. E.; Bent, S. F.; Wilson, W. L.; Schilling, M. L.; Ungashe, S. B. *J. Am. Chem. Soc.* **1994**, *116*, 6631−6635.

(18) Nüesch, F.; Moser, J.-E.; Shklover, V.; Grätzel, M. *J. Am. Chem. Soc.* **1996**, *118*, 5420−5431.

(19) Campus, F. Unpublished data, Ph.D. Thesis, EPFL.

(20) (a) Bard, A. J.; Ledwith, A.; Shine, H. J. *Adv. Phys. Chem.* **1976**, *13*, 155−278. (b) Dapperheld, S.; Steckhan, E.; Grosse Brinkhaus, K. H.; Esch, T. *Chem. Ber.* **1991**, *124*, 2557−2567. (c) Steckhan, E. *Top. Curr. Chem.* **1987**, *142*, 3−69.

(21) Bonhôte, P.; Dias, A. P.; Papageorgiou, N.; Kalyanasundaram, K.; Grätzel, M. *Inorg. Chem.* **1996**, *35*, 1168−1178.

(22) Bard, A. J.; Faulkner, L. R. *Electrochemical Methods, Fundamental and Applications;* J. Wiley: New York, 1980; pp 535−536.

(23) The absorbance of the electrode measured after chemical oxidation by $NOBF_4$ was proportional to the molar fraction $x_1$ in the mixed monolayer, with a correlation coefficient of 0.992 over seven points.

(24) (a) Sahimi, M. *Application of Percolation Theory*; Taylor & Francis: London, 1994; pp 1−22. (b) Bunde, A., Havlin, S., Eds. *Fractal and Disordered Systems*; Springer: Heidelberg, 1991; pp 59−171.

(25) (a) Miller, J. R.; Beitz, J. V. *J. Chem. Phys.* **1981**, *74*, 6746−6756. (b) Miller, J. R.; Beitz, J. V.; Huddleston, R. K. *J. Am. Chem. Soc.* **1984**, *106*, 5057−5068.

(26) Heimer, T. A.; D'Archangelis, S. T.; Farzad, F.; Stipkala, J. M.; Meyer, G. J. *Inorg. Chem.* **1996**, *35*, 5319−5324.

(27) Bock, C. R.; Connor, J. A.; Gutierrez, A. R.; Meyer, T. J.; Whitten, D. G.; Sullivan, B. P.; Nagle, J. K. *Chem. Phys. Lett.* **1979**, *61*, 522−525.

(28) Chan, M. S.; Wahl, A. C. *J. Phys. Chem.* **1982**, *86*, 126.

(29) (a) Bock, C. R.; Connor, J. A.; Gutierrez, A. R.; Meyer, T. J.; Whitten, D. G.; Sullivan, B. P.; Nagle, J. K. *Chem. Phys. Lett.* **1979**, *61*, 522−525. (b) Grampp, G.; Jaenicke, W. *Ber. Bunsen-Ges. Phys. Chem.* **1984**, *88*, 335−340.

(30) Debye, P. *Trans. Electrochem. Soc.* **1942**, *82*, 265−272.

(31) Noyes, R. M. *Prog. React. Kinet.* **1961**, *1*, 129−160.

(32) (a) de Schryver, F. C.; Boens, N.; Put, J. *Adv. Photochem.* **1977**, *10*, 359−465. (b) de Schryver, F. C.; Collart, P.; Vandenriessche, J.; Goedeweeck, R.; Swinnen, A. M.; Van der Auweraer, M. *Acc. Chem. Res.* **1987**, *20*, 159−166. (c) Borkent, J. H. Dissertation, Universiteit van Amsterdam, 1976.

(33) (a) Chidsey, C. E.; Feldman, B. J.; Lundgren, C.; Murray, R. W. *Anal. Chem.* **1986**, *58*, 601−607. (b) Natan, M. J.; Wrighton, M. S. *Prog. Inorg. Chem.* **1989**, *37*, 391−494.